Article

Current Biology

Role of Synchronous Activation of Cerebellar Purkinje Cell Ensembles in Multi-joint Movement Control

Highlights

- *tg/tg* mice show affected swing duration and phase coupling of limb movements
- PCs in ataxic *tg/tg* mice show delayed and reduced complex spike (CS) co-activation
- At rest, simple spike (SS) co-activation can elicit preferred locomotion sequences
- During locomotion, SS co-activation can be correlated with gait-inhibition patterns

Authors

Tycho M. Hoogland, Jornt R. De Gruijl, ..., Cathrin B. Canto, Chris I. De Zeeuw

Correspondence

hoogland@nin.knaw.nl

In Brief

It is unknown to what extent Purkinje cell ensemble coding is relevant for locomotion. Using two-photon calcium imaging and optogenetics in combination with a novel disk treadmill, Hoogland et al. show that co-activity of both complex spikes and simple spikes within Purkinje cell ensembles may contribute to coordination of multi-joint movements.

Hoogland et al., 2015, Current Biology *25*, 1157–1165
May 4, 2015 ©2015 The Authors
http://dx.doi.org/10.1016/j.cub.2015.03.009

CellPress

Current Biology
Article

Role of Synchronous Activation of Cerebellar Purkinje Cell Ensembles in Multi-joint Movement Control

Tycho M. Hoogland,[1,3,*] Jornt R. De Gruijl,[1,3] Laurens Witter,[1] Cathrin B. Canto,[1] and Chris I. De Zeeuw[1,2]
[1]Netherlands Institute for Neuroscience, Royal Netherlands Academy of Arts and Sciences, Meibergdreef 47, 1105 BA Amsterdam, the Netherlands
[2]Department of Neuroscience, Dr. Molewaterplein 50, Erasmus MC, 3015 GE Rotterdam, the Netherlands
[3]Co-first author
*Correspondence: hoogland@nin.knaw.nl
http://dx.doi.org/10.1016/j.cub.2015.03.009
This is an open access article under the CC BY-NC-ND license (http://creativecommons.org/licenses/by-nc-nd/4.0/).

SUMMARY

It is a longstanding question in neuroscience how elaborate multi-joint movements are coordinated coherently. Microzones of cerebellar Purkinje cells (PCs) are thought to mediate this coordination by controlling the timing of particular motor domains. However, it remains to be elucidated to what extent motor coordination deficits can be correlated with abnormalities in coherent activity within these microzones and to what extent artificially evoked synchronous activity within PC ensembles can elicit multi-joint motor behavior. To study PC ensemble correlates of limb, trunk, and tail movements, we developed a transparent disk treadmill that allows quantitative readout of locomotion and posture parameters in head-fixed mice and simultaneous cellular-resolution imaging and/or optogenetic manipulation. We show that PC ensembles in the ataxic and dystonic mouse mutant *tottering* have a reduced level of complex spike co-activation, which is delayed relative to movement onset and co-occurs with prolonged swing duration and reduced phase coupling of limb movements as well as with enlarged deflections of body-axis and tail movements. Using optogenetics to increase simple spike rate in PC ensembles, we find that preferred locomotion and posture patterns can be elicited or perturbed depending on the behavioral state. At rest, preferred sequences of limb movements can be elicited, whereas during locomotion, preferred gait-inhibition patterns are evoked. Our findings indicate that synchronous activation of PC ensembles can facilitate initiation and coordination of limb and trunk movements, presumably by tuning downstream systems involved in the execution of behavioral patterns.

INTRODUCTION

The cerebellum is essential for the proper coordination of locomotion and posture [1–4]. To achieve optimal spatiotemporal control of the multiple motor domains involved in these complex behaviors, the cerebellum must orchestrate select repertoires of motor synergies through projections to the spinal cord [5–7] and cerebral cortex [8] via the brainstem and thalamus, respectively. Accordingly, when the integrity of the cerebellar circuit is perturbed, motor output is severely impaired, often resulting in ataxia and dystonia [9]. The cerebellum receives its main inputs from the inferior olive, which project to the Purkinje cells (PCs) via climbing fibers (CFs), and from several brainstem nuclei, which provide PCs with mossy fiber (MF)-parallel fiber (PF) afferents via the granule cells [10]. The interaction between these two orthogonally oriented, afferent systems is critical for cerebellar motor coordination, including that of locomotion and posture [11]. Whereas the MF-PF system has a strong impact on the amplitude of the simple spike (SS) modulation of PCs, the CF system and its afferents determine not only the phase and amplitude of the modulation of the complex spikes (CSs), but also the phase of the SS modulation [12]. Importantly, CFs are organized in modules projecting to narrow rostro-caudal (micro)zones of PCs in the cerebellar cortex. PCs within a (micro)zone in turn converge on cerebellar nuclei (CN) neurons, through which the cerebellum exerts its excitatory control of premotor nuclei [13, 14] and inhibitory feedback to the inferior olive [15]. The olivocerebellar modules may thus control specific muscle synergies that guide complex movements [16, 17]. Indeed, synchronicity of CF inputs, which depends on electrotonic coupling and intrinsic oscillatory properties of olivary neurons [18], may dynamically control motor output [4].

Two-photon microscopy has enabled cellular-resolution readout of dozens to hundreds of neighboring PCs in awake behaving mice [19–22]. CS co-activation rates have been shown to be elevated during locomotion [20]. However, it remains to be clarified to what extent synchronous PC activity is corrupted in movement disorders [23]. It is therefore important to resolve whether aberrant patterns of CS activity occur in animal models of ataxia and dystonia, whether potential abnormalities in the delays of ensemble activity can be correlated to deficits in locomotion and posture, and to what extent manipulation of activity patterns can influence limb and trunk movements. Here, we sought to tackle these questions exploiting the direct readout of the behavior of all limbs and tail with a newly developed transparent-disk-based treadmill. The disk treadmill enabled the stable imaging and optogenetic manipulation of PC ensembles

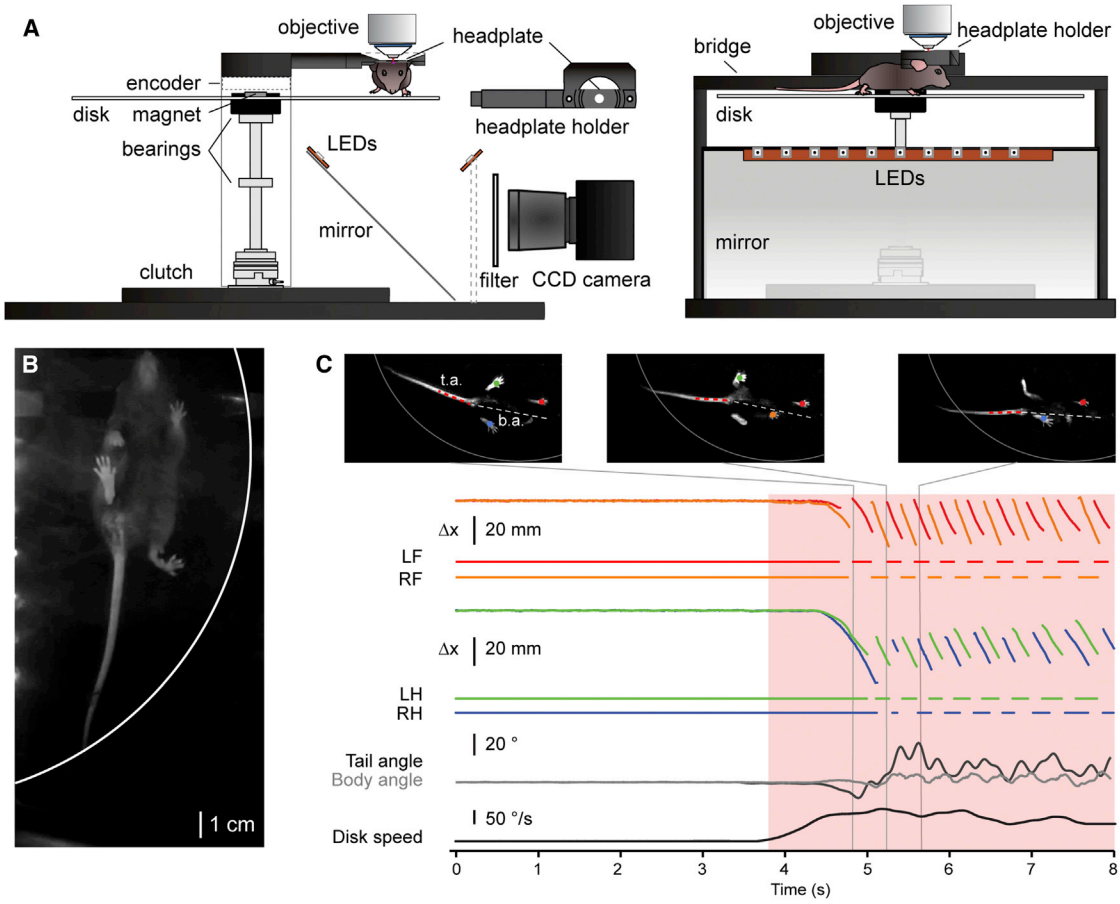

Figure 1. A Transparent Disk Treadmill

(A) Mice with head posts are mounted in a head post holder that is attached to a central bridge overlaying a rotary transparent Plexiglas disk on which they can walk at will due to low-friction ball bearings and low disk inertia. A mirror placed underneath the disk reflects an image of the mouse as seen from below onto an infrared-sensitive CCD camera. The mouse is illuminated by two strips of LEDs (940 nm), with one mounted on the mirror and the other directly opposite, both at 45° angles. An optical filter placed between the mirror and camera blocks light from two-photon laser excitation during imaging sessions or optogenetic stimulation while passing light used for illumination of the mouse. A magnetic encoder centered above the disk in conjunction with a magnet placed in the center of the rotary disk allows recording of disk position as a voltage signal. A computer-controlled electromagnetic clutch placed along the rotational axis can be engaged for brief durations to generate high saliency sensory perturbations.

(B) Image of a mouse as captured by the CCD camera (disk edge indicated in white).

(C) Top: frames taken during different phases of mouse locomotion. Paws are indicated by the colored dots overlaid on each frame, while body axis (b.a.) and tail axis (t.a.) are indicated by the white and red dashed lines, respectively. Bottom: x displacement of the four paws of a mouse are represented in colors corresponding to the identified paw objects in the top panels with directly below the state vectors representing paw stance and swing periods. Vertical gray lines denote the time points during locomotion that correspond to the frames shown in the top panels. LF, left front limb; RF, right front limb; LH, left hind limb; RHL, right hind limb.

See also Figure S1.

in head-fixed mice not only at rest, but also during self-initiated or sensory perturbation-evoked, reflexive limb and trunk movements. We applied the disk treadmill to study the behavior of the ataxic and dystonic mouse mutant *tottering* (*tg/tg*), which suffer from a P/Q-type calcium channel mutation [24–27]. We find that their aberrant locomotion and posture are correlated with reduced levels and delayed timing of PC CS co-activation within cerebellar microzones. Using optogenetics to evoke SS activity simultaneously in multiple PCs [28], we show that a variety of movement patterns can be elicited contingent on the behavioral state of the animal. Taken together, our data provide evidence that PC ensembles contribute to on-the-fly control of coordination and posture, with manipulations of these cell assemblies resulting in altered motor repertoires.

RESULTS

Disk Treadmill and Quantification of Motor Behavior

A transparent disk treadmill was developed to register movements of trunk, tail, and all limbs in head-fixed awake mice while allowing stable access for cellular resolution circuit imaging or optogenetic stimulation. Additionally, sensory perturbations could be presented by engaging a magnetic clutch placed along the rotational axis of the disk (Figure 1A) to trigger

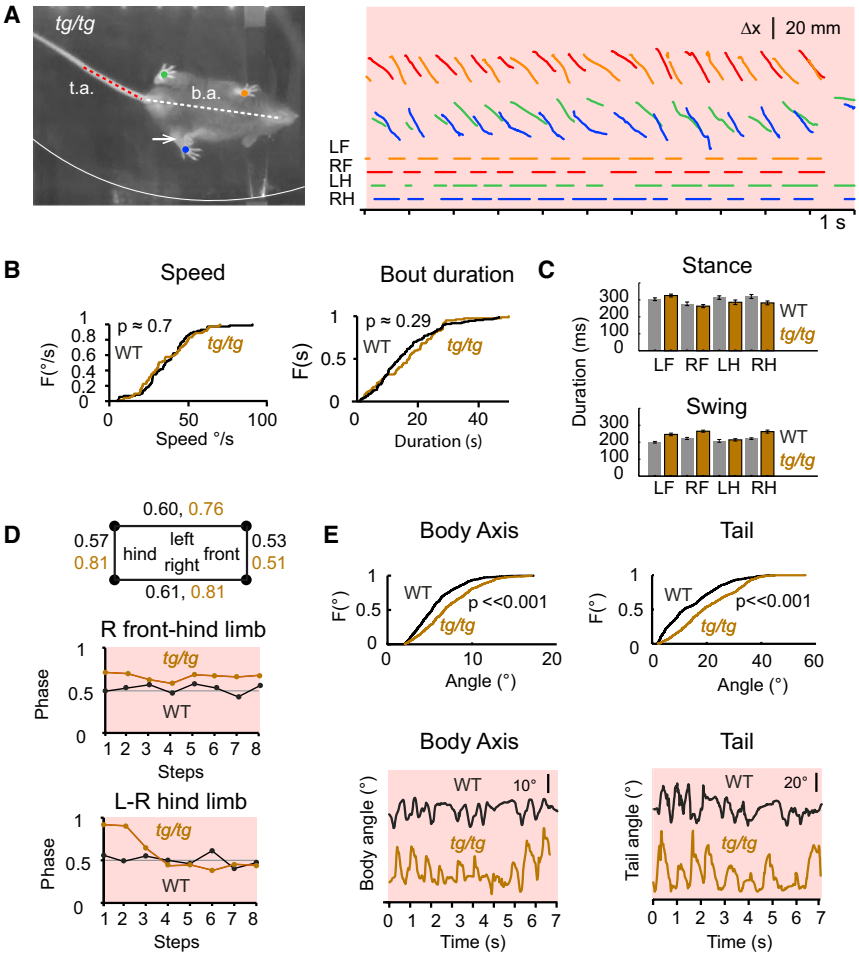

Figure 2. Motor Deficits in *tg/tg* Mice Analyzed with a Disk Treadmill

(A) Left: body (b.a.) and tail (t.a.) axis and paw positions (colored dots) extracted from a *tg/tg* mice walking on the transparent disk treadmill. The white arrow denotes a misstep. Right: paw displacements (in x) and corresponding gait patterns in a *tg/tg* mouse.

(B) Cumulative frequency histograms of treadmill speed (top) and running bout duration (bottom) in wild-type and *tg/tg* mice. Both were not significantly different (speed, p = 0.7; bout duration, p = 0.29).

(C) Stance and swing times for wild-type and *tg/tg* mice (mean ± SEM).

(D) Coupling between limbs shows deficits in *tg/tg* mice. Examples are shown of the increased out-of-phase placement of limbs in *tg/tg* relative to wild-type mice.

(E) Body and tail angles showed significantly larger deflections in *tg/tg* than in wild-type mice.

See also Figure S2.

spino-cerebellar and other reflexes associated with strong CS co-activation [19]. Paw, body, and tail movements were detected by recording the mouse with an infrared-sensitive charge-coupled device (CCD) camera from below via a mirror placed at a 45° angle (Figure 1B). Animals were illuminated by two strips of infrared light-emitting diodes (LEDs), one mounted on the mirror and another one across from it on a custom post. A magnetic encoder placed above the disk in conjunction with a magnet placed in the center of the rotating disk allowed logging of disk position as a voltage signal (Figure 1A). For reliable detection of multi-limb gait and posture, camera frames were denoised and background subtraction was performed prior to paw and tail segmentation. Objects were classified based on position, size, and orientation using a three-layer feedforward neural network (Figure 1C). This network was trained by assigning objects to any of six classes: left hind paw, left front paw, right hind paw, right front paw, tail, or none. Subsequently, paw coordinates were used to extract gait parameters, whereas trunk axis and tail angles were determined to assess parameters pertaining to posture (Figure 1C; Supplemental Experimental Procedures).

Phenotyping Locomotion and Posture Behavior in *tg/tg* Mice

We investigated locomotion patterns, posture, and fine paw motor behavior of adult *tg/tg* mice (n = 4; weight 20.23 ± 1.5 g) and wild-type littermates (n = 4; 23.5 ± 2.9 g) using the disk treadmill (Figures 2A–2E). Coordination deficits and ataxia could be readily observed by the naked eye in that stepping of hind limbs onto front limbs occurred in *tg/tg* mice, but not wild-types (Figure 2A). Yet, average locomotion speeds did not differ significantly between genotypes (36.4° ± 15.6° per second for wild-type and 35.7° ± 15.6° per second for *tg/tg*; p = 0.70, two-sample Kolmogorov-Smirnov [K-S] test) and bouts of locomotion had similar overall duration in wild-type and *tg/tg* mice (16.9 ± 10.3 s and 16.2 ± 10.9 s, respectively; p = 0.29, two-tailed t test) (Figure 2B). Moreover, average duration of stance also did not differ among genotypes (p = 0.16, Kruskal-Wallis test) (Figure 2C). In contrast, average duration of swing of *tg/tg* mice was significantly longer ($p = 1.3 \times 10^{-11}$, Kruskal-Wallis test) than that in wild-type mice (Table S1), (Figure 2C).

To quantify to what extent coordination was affected, we looked at phase coupling between limbs (Figure 2D). Phase values were calculated by taking the difference between the stance start of the first and second limb and dividing this by the step cycle duration of the second limb, rendering the value of 0.5 as a close approximation of optimal limb alternation [29]. Significant deviations point toward limb placements that are inappropriately out of phase. A multivariate comparison of deviations from normal limb alternation (absolute deviation from 0.5) revealed that overall limb coupling in wild-type and *tg/tg* mice was significantly different (p = 0.003, Kruskall-Wallis test). Post hoc individual comparisons indicated that hind limbs (wild-type, 0.57 ± 0.1; *tg/tg*, 0.81 ± 1.0; p = 0.006, two-sample K-S test), left limbs (wild-type, 0.62 ± 0.2; *tg/tg*, 0.76 ± 0.5; p = 0.002), and right limbs (wild-type, 0.61 ± 0.2; *tg/tg*, 0.81 ± 0.6; p = 0.03), but somewhat less so front limbs (wild-type, 0.54 ± 0.1; *tg/tg*, 0.51 ± 0.1; p = 0.07), were unduly out of phase in

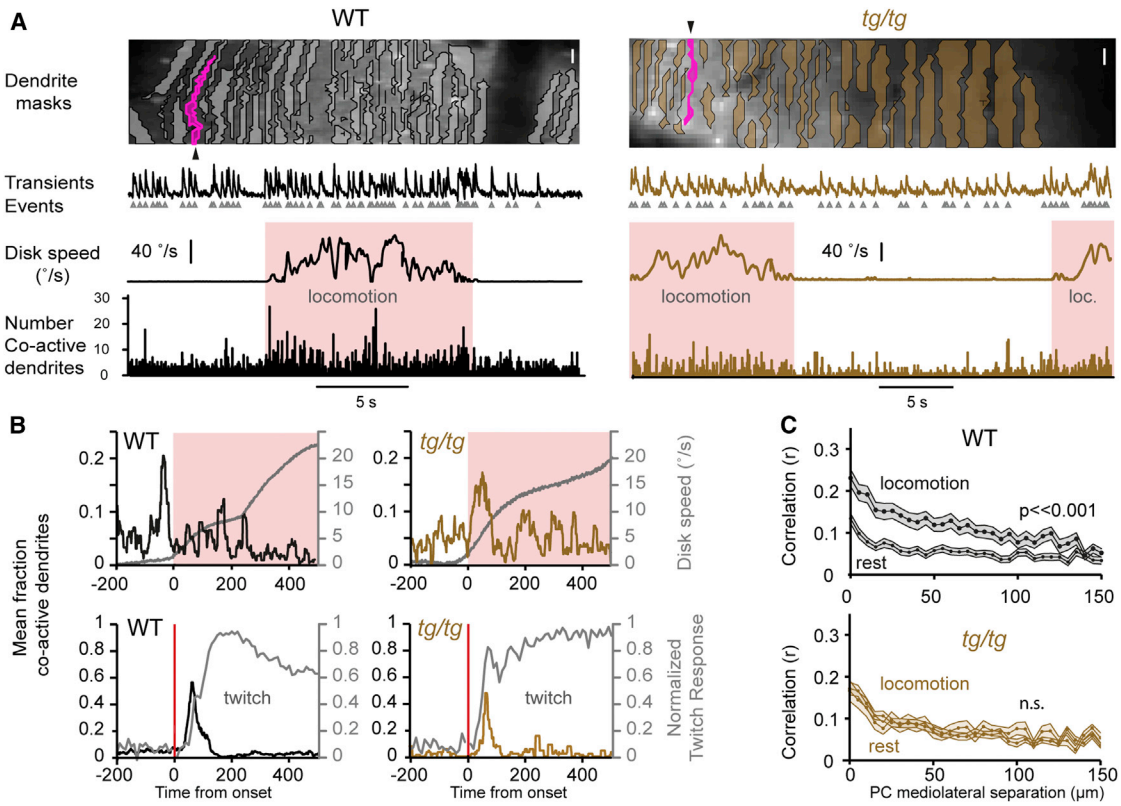

Figure 3. Altered Timing and Reduced Levels of Locomotion-Associated Microzonal CS Co-activation in *tg/tg* Mice

(A) Two-photon optical sections of the cerebellar cortex bolus-loaded with OGB-1/AM with superimposed PC dendrite masks extracted with spatial independent component analysis (scale bar, 10 μm). Traces from the bright dendrite (pink) and extracted CS events (gray triangles) are shown for both wild-type and *tg/tg* mice together with disk encoder speed and the number of PC dendrites with co-active CS events.

(B) Synchronous CS events as triggered by locomotion onset. Co-active events were binned with ms precision using a hyperacuity algorithm. In *tg/tg* mice, peak event synchrony was delayed relative to wild-types with respect to locomotion onset. When CS co-active events were triggered off of sensory perturbations evoked with the magnetic clutch of the disk treadmill (red lines), elicited twitches resulted in similarly timed CS synchrony.

(C) Spatial correlations of CS events in wild-type mice showed increased correlation during locomotion. Such correlation increases were not observed in *tg/tg* mice during locomotion. Shaded regions indicate the SEM.

See also Figure S3.

tg/tg mice (Figure 2D). Along the same line, during locomotion, body-axis and tail angles in *tg/tg* mice showed significantly larger deflections ($p = 7.2 \times 10^{-15}$ and $p = 4.5 \times 10^{-21}$, respectively; two-sample K-S test) than those in wild-types (*tg/tg* tail angle 20.5° ± 10.6° and body-axis angle 7.2° ± 3.2°; wild-type tail angle 14.4° ± 9.9° and body-axis angle 5.7° ± 2.6°), (Figures 2E and S2). Thus, coordination between limbs, as well as coordination between trunk and tail, was altered in *tg/tg* mice.

Correlating Motor Behavior with CS Activity in Microzones

Given the prolonged swing duration and impaired coordination of *tg/tg* mice during locomotion, we next set out experiments to find correlations between changes in cellular-resolution activity of PC ensembles and differences in motor performance parameters. We performed two-photon imaging of PCs in vermis lobule V on the disk treadmill during both rest and locomotion (Figure 3A). Calcium transients evoked by CSs in PC dendrites (field size 266.6 ± 39.7 μm; 23.8 ± 9.7 dendrites/field) could be readily imaged in wild-type mice (n = 4 mice, 630 dendrites) and *tg/tg* mice (n = 3 mice, 192 dendrites). In *tg/tg* mice, CS-evoked transients had significantly reduced amplitudes compared to those in wild-type littermates (Table S2), possibly reflecting a reduced calcium influx through the mutated P/Q-type calcium channels [27]. Nevertheless, CS rates in *tg/tg* mice at rest were higher than those in wild-types (1.26 ± 0.4 Hz in *tg/tg* versus 1.13 ± 0.4 Hz in wild-type; p = 0.001, two-sample K-S test). Likewise, during locomotion, CS rates were moderately yet significantly increased in *tg/tg* mice (1.52 ± 0.3 Hz in *tg/tg* versus 1.43 ± 0.3 Hz in wild-type; $p = 7.9 \times 10^{-7}$, two-sample K-S test). Given the longer swing duration in *tg/tg* mice, we hypothesized that the timing of CS co-activation may be delayed with respect to their motor behavior. We applied a custom hyperacuity algorithm to increase the sampling resolution of CS co-activation events to 1 kHz [19]. In a 200-ms window centered around locomotion onset, the average peak fraction of co-active PC dendrites in *tg/tg* mice was significantly reduced (0.16 ± 0.0 in *tg/tg* versus 0.21 ± 0.1 in wild-type; p = 0.02, two-sample K-S test), and their peak CS co-activation responses were delayed significantly by 86.9 ± 12.6 ms ($p = 1.4 \times 10^{-16}$, *tg/tg* versus

wild-types; signed-rank test). Indeed, whereas peak CS co-activation in wild-types preceded the onset of the disk movement, that in *tg/tg* occurred after it (Figure 3B).

In addition, the overall rate of co-active CS events in *tg/tg* mice during a locomotion bout (0.12 ± 0.03 co-active events per second) was significantly lower (p = 0.02) than that in wild-type mice (0.31 ± 0.27 co-active events per second); in fact, over distances encompassing multiple cerebellar microzones, pairwise correlation distributions in *tg/tg* mice during locomotion were indistinguishable from those during rest (for comparison across 150 μm, 5 μm bin interval, p = 0.2, Kruskal-Wallis test), whereas they were significantly increased during locomotion in wild-type mice (for comparison across 150 μm, 5 μm bin interval, $p = 1.3 \times 10^{-8}$, Kruskal-Wallis test) (Figure 3C). Thus, despite a moderate increase of CS rate during locomotion, CS synchrony was significantly disrupted during self-initiated locomotion in *tg/tg* mice. By contrast, *tg/tg* peak co-activation of PCs in response to sensory perturbations evoked by the magnetic clutch of the disk treadmill showed similar delays (53.7 ± 4.1 ms in *tg/tg* versus 50.4 ± 5.9 ms in wild-type; p = 0.9, two-sample K-S test). Moreover, there was no significant difference (p = 0.15, two-sample K-S test) between the latency periods of peak deviations in the differentials of the temporal twitch profiles in *tg/tg* mice (51.8 ± 13.6 ms) and those in wild-types (62 ± 12.9 ms), while the corresponding peak levels of CS synchrony in *tg/tg* mice were also similar to those in wild-types during this paradigm (0.49 ± 0.2 in *tg/tg* versus 0.55 ± 0.26 in wild-type; p = 0.89, two-sample K-S test).

State-Dependent Effects on Motor Behavior of Selective Optogenetic Induction of SS Activity in PC Ensembles

Since granule cell layer activity has also been shown to be increased around locomotion onset [20], we next explored the impact of SS modulation of PC ensembles on sequences of limb, trunk, and tail movements during periods of rest and locomotion using optogenetic stimulation in vermis lobule V of awake mice. PCs expressing ChR2(H134R)-eYFP driven by PCP2-Cre [30] were stimulated using optical fibers implanted above lobule V (Figures 4A and 4B). We used up to 3 mW output power (i.e., ~24 mW/mm^2 at the cerebellar surface), which in whole-cell recordings in vivo elicits SS activity without a depolarization block [28]. Optogenetic stimulation (1–3 mW, 250 ms) resulted in stereotyped behavior that fell into different classes, depending on the state of the animal at the time of stimulation (Figure 4C). At rest, movements were readily evoked (98.7% response, 1.3% no response) and consisted of whole-body or tail twitches (71.6%, 373/521 stimulations, n = 7 mice; Movie S1) or initiation of stepping (27.3%, 142/521, n = 7; Movie S2), whereas during locomotion responses were less frequently evoked (70% response, 30% no response) and consisted mainly of halting (38.1%, 98/257, n = 7; Movie S3) or slowdown of locomotion (31.9%, 82/257, n = 7). The whole-body twitches following stimulations at rest could be evoked with stimulus durations as short as 10 ms (Figure S3), and independent from stimulus duration they occurred at a rather fixed latency of approximately 75 ms after stimulus offset (e.g., 74.9 ± 38.7 ms after offset for 372 stimuli at 250 ms duration, n = 4 mice; see [28]) (Figure S3). By contrast, initiation of stepping following stimulations at rest (i.e., 250 ms) usually (77%) started before stimulus offset (Figures 4D); treadmill speed began to increase at 209.9 ± 49.3 ms from stimulus onset (range 95–311 ms, 100 onsets, n = 3 mice) and peaked bimodally at 315 and 445 ms (p = 0.02, Hartigan's dip test) [31]. Most of the step-inducing optogenetic stimulations (114, n = 3 mice) resulted in four distinct limb movements in succession (78.1%, 89/114; as opposed to 12.3% and 9.6% for three and two consecutive displacements, respectively). Considering the stimulations with four consecutive displacements, two particular sequences of displacements occurred in a predominant fashion (Figure 4H): LF-RH-RF-LH (36.0%, 32/89) and RF-LH-LF-RH (20.2%, 18/89) (L, R, F, and H indicate left, right, front, and hind limb, respectively). The preferred sequences of these light-evoked stepping patterns were similar to those initiated spontaneously (n = 4 mice) in that the LF-RH-RF-LH (16%) and RF-LH-LF-RH (25%) sequences were also the most frequent ones during self-initiated locomotion, suggesting that the optogenetic stimulation induced a natural type of motor behavior. Stimuli of shorter durations (e.g., 50 ms) could trigger locomotion as well, but here movements started on average 132.7 ± 20.4 ms after stimulus onset (52 stimuli, n = 3 mice) (Figure S3); yet again, the main preferred patterns consisted of LF-RH-RF-LH (35%, 17/52) and RF-LH-LF-RH (29%, 15/52). Instead, optogenetic stimulation during locomotion usually caused mice to counteract locomotion affecting gait patterns of all four limbs (Figures 4D–4G). In cases of a standstill, disk speed began to decline at 226.5 ± 125.2 ms (44 terminations, n = 5 mice) after onset of a 250-ms stimulus and came to a complete standstill after 479.9 ± 142.7 ms (range 233–904 ms). The jitter (i.e., 142.7 ms) around the termination point was not correlated with average locomotion speed in the 500 ms preceding stimulus onset ($R^2 = 0.003$, *F* statistic = 0.16, p = 0.69). In cases of slowdown of locomotion, a similar time profile was seen as when animals came to a complete halt. Here speed began to decline at 205.8 ± 151.6 ms (27 slowdowns, n = 5 mice). The speed prior to either a complete halt or slowdown of locomotion was not significantly different (halt versus slowdown 63.3° ± 27.1° per second and 68.2° ± 23.7° per second; p = 0.42, two-tailed t test) and is therefore unlikely to determine the time point of movement cessation when ensembles of PCs were stimulated. In contrast, optogenetic stimulation (for up to 2 s) of PCs of the floculus of the vestibulocerebellum or the lateral cerebellar hemispheres did not evoke complex locomotion patterns (data not shown). Thus, using the disk treadmill, we deciphered complex walking patterns with preferred sequences of limb placements following optogenetic induction of SS activity of ensembles of PCs at rest, and, likewise, we monitored various gait-inhibition patterns when PCs were activated during locomotion.

DISCUSSION

The transparent disk treadmill allowed us to improve readout of various aspects of cerebellum-dependent motor behavior including gait, posture, and small limb movements, advancing upon previous treadmill systems that also permit concurrent readout of neural circuits and behavioral state [32], but not more detailed aspects of complex movements. By imaging ensembles of PCs in awake behaving mice on this disk treadmill, we could study microcircuit level changes of spatiotemporal

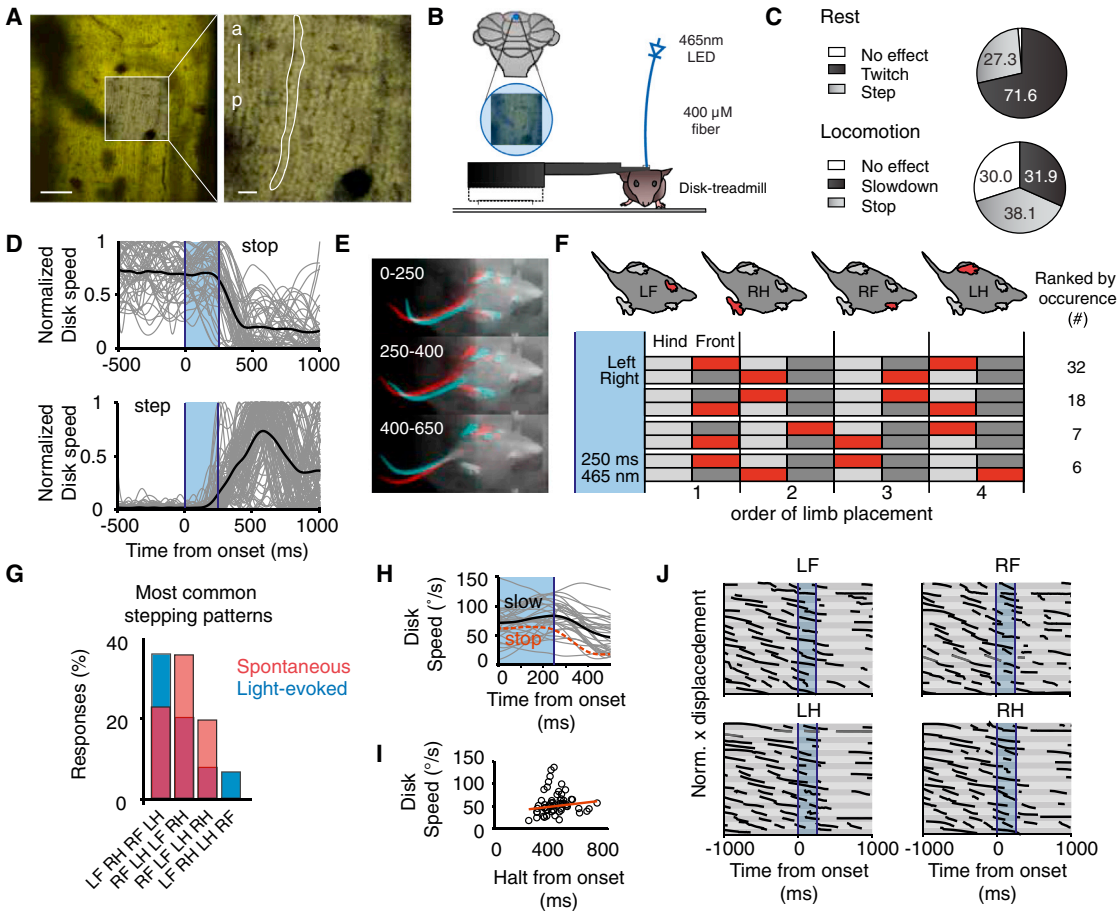

Figure 4. State-Dependent Motor Behavior during Selective Optogenetic Activation of PCs

(A) Left: optical section of the molecular layer of the cerebellum acquired with a two-photon microscope indicating the presence of the ChR2(H134)-EYFP fusion protein. Right: closeup of the boxed region shows expression of ChR2(H134)-EYFP in sagitally arranged PC dendrites (the outline denotes a single arbor; a, anterior; p, posterior).

(B) Schematic indicating the region of optogenetic stimulation (lobule V). Mice were mounted on the treadmill, and a 400 µm fiber was mounted above a small craniotomy above the medial cerebellar vermis lobule V for PC stimulation. A blue LED acted as light source and was coupled into the fiber giving a mean output of 1–3 mW at the fiber tip.

(C) Optogenetic stimulation of PCs (250 ms, 465 nm; shaded blue areas) in behaving mice resulted in stereotyped behaviors that were state dependent. Stimulation during rest could evoke twitches (see also Figures S3A and S3B) or initiate stepping behavior, whereas stimulation during the step cycle could slow down or stop locomotion.

(D) Treadmill disk speeds (normalized, individual traces, gray; average response, black) showing halting (top) or initiation (bottom) of locomotion when PCs are optogenetically stimulated.

(E) Camera frame differences at three time intervals following optogenetic stimulation offset demonstrating that PC stimulation during rest triggered stepping on the disk treadmill.

(F) The four most common stepping patterns are depicted in red and illustrate the placement order of each paw for a sequence of four steps.

(G) Optogenetically induced and spontaneous walk patterns were comparable in that most frequently a front paw was first lifted followed by a diagonally apposed hind limb.

(H) Disk speeds during slowdown of locomotion (individual traces, gray; average response, black) compared to average response during halting of locomotion (red). Speeds did not differ significantly prior to slowdown or halting of locomotion.

(I) Speed during spontaneous walking prior to the stimulus onset does not determine the timing of when the animal comes to a complete halt.

(J) PC stimulation during locomotion causes interruption of the step cycle. Shown are trials of normalized paw displacements (in x) for three mice triggered off of the onset of a 250 ms light stimulus.

See also Movies S1, S2, and S3.

CS activity and their behavioral correlates in a mouse model of ataxia and dystonia. Abnormalities of CS activity of PC ensembles in cerebellar microzones of *tg/tg* mice co-occurred with deficits in timing and coupling of limb coordination and posture. In addition, we showed that optogenetically evoked SS activity in ensembles of PCs can influence the sequence and timing of limb and trunk movements both at rest and during locomotion. Thus, the output of cerebellar (micro)zones, in concert with other downstream regions, contributes to coordination of multi-joint- and multi-limb-mediated movements.

Timing of cerebellar output is essential for proper coordination [33]. Whereas in wild-types CS co-activity in vermis lobule V preceded self-initiated movements as detected by disk speed, in *tg/tg* mice it occurred after locomotion initiation. More specifically, we found in *tg/tg* mice that in a 200-ms window centered around onset of locomotion the average peak fraction of co-active PC dendrites was significantly reduced and that their peak CS co-activation responses were delayed by approximately 87 ms. When considering the complete period of a locomotion bout, throughout which phase coupling of limbs was affected continuously, the overall rate of co-active CS events in *tg/tg* mice was not even significantly different from that at rest. A similar phenotype occurs in knockouts of connexin36, in which CS co-activation is attenuated concomitantly with altered limb and tail reflex responses following perturbations [19]. Together, these data suggest that attenuation and delay of CS co-activation within cerebellar microzones can contribute to changes in the timing and execution of both complex and reflex movements.

How can the abnormal CS patterns during locomotion in *tg/tg* mice be explained? Given that synchronous activation of PCs in response to sensory perturbations evoked by the treadmill magnetic clutch showed similar delays to peak co-activation in *tg/tg* and wild-type mice, our data suggest that it is not a difference in the sensory inputs to the olive or related phase resetting [34–36], but rather a result of altered dynamic processing in the olivocerebellar modules. Several other findings also point this way. First, there was a general increase in CS firing during both rest and locomotion in *tg/tg* mice, which causes a reduction of SS activity [37] and thereby activation of CN neurons that inhibit the inferior olive. This effect will even be enhanced by the increased noise level in SS activity of *tg/tg* mice, reducing the impact of SS activity on CNs [38]. Second, activity increases in CNs that inhibit olivary neurons are in line with a reduced potential for CS co-activation, because this inhibitory input, which is strategically located next to the gap junctions in the olivary glomeruli [15], can decouple olivary cells presumably through shunting mechanisms [39, 40]. Thus, when SS activity and CN activity are taken into account, all findings on CS activity in *tg/tg* mice during locomotion can be explained by mechanisms that control activity within the olivocerebellar loop.

The finding that movement onset in *tg/tg* occurred before co-activation of CSs supports the possibility that these self-initiated movements occurred through concerted action of other brain regions without initial involvement of the cerebellum. Alternatively, SS co-activity might have also contributed to movement initiation. Indeed, optogenetic stimulation of PC ensembles in vermis lobule V, which drives their SS activity [28], triggered behavior of limbs, trunk, and tail depending on the state of the animal. At rest, responses consisted of posture twitches or complex walking patterns, whereas during locomotion, various forms of gait inhibition occurred. Given that the walking patterns elicited by optogenetic stimulation produced natural sequences of limb movements that also occurred during spontaneous locomotion, it is likely that the zonal stimulation of ensembles in vermis lobule V triggered motor programs embedded downstream in brainstem and spinal cord [6].

The locomotion patterns we observed after optogenetic stimulation of PC ensembles are distinct from those generated by stimulation of striatum or cerebral cortex using comparable stimulus durations [41, 42]. Optogenetic activation of the direct and indirect striatal pathways to the thalamus increase and decrease velocity of limb movements, respectively. Likewise, optogenetic stimulation of limb regions in the motor cortex induces relatively simple, time-locked movements that allow mapping of distributions of neurons associated with individual limb movements [42]. Thus, although the numbers of neurons stimulated in these latter studies probably differed, it should be noted that an SS firing increase in an ensemble of PCs after optogenetic stimulation for only a few tens of milliseconds at moderate stimulation intensity can be sufficient to elicit quite elaborate locomotion patterns. Future experiments should address to what extent SS activity of ensembles of PCs interacts with that of CS activity to facilitate or inhibit movements, e.g., by using optogenetic stimuli timed to a particular phase of the olivary oscillation [35, 36, 43] and/or by sequentially stimulating different CF zones along the medio-lateral extent of the cerebellum. In addition, it will be interesting to find out how the output of the cerebellum, i.e., the cerebellar nuclei, can exactly tweak the downstream regions to control the coordination of complex multi-joint movements.

EXPERIMENTAL PROCEDURES

Mouse Surgery

All experiments adhered to the European guidelines for the care and use of laboratory animals (Council Directive 86/6009/EEC) and were approved by the animal experiment committee of the Royal Netherlands Academy of Arts and Sciences (DEC-KNAW). For imaging experiments, data were collected from *tg/tg* mice and wild-type littermates (C57BL/6J background; Jackson Laboratory). A custom stainless-steel plate was attached to the mouse skull (midline, 2 mm posterior of lambda), after a small skin incision, using dental cement (Super Bond C&B, Sun Medical). This plate had a circular cutout of 8-mm and a recessed rim of 1-mm width, allowing a round 8-mm diameter cover glass (thickness 0.15 mm; Warner Instruments, catalog number CS-8R) to lie flush with the plate surface. A custom clamp was used to exert additional pressure on the cover glass after 2% agarose (type III-A; Sigma-Aldrich) or Kwik-Sil (World Precision Instruments) application to stabilize the brain during imaging. With these measures, axial motion artifacts were kept to a minimum during imaging sessions (Figure S4). Surgeries were performed under anesthesia with isoflurane (2%, IsoFlo; Abbott) in a stereotactic frame with mice placed on a temperature-controlled (TC-1000; CWE) heating mouse pad with thermistor (YSI-451; CWE) to maintain a constant body temperature of 37°C. Eye ointment (Terra-Cortril; Pfizer) was applied to keep the eyes moist. Xylocaine (lidocaine-HCL, 10%; Astra Zeneca) was applied to the incision site and wound areas.

Disk Treadmill

The disk treadmill consisted of a transparent disk (thickness 2 mm, diameter 260 mm) made of poly (methyl methacrylate) secured on an axis with low-friction ball bearings (SKF Explorer Bearing 608). Rotation was measured with a magnetic encoder (RFC 4801-636-111-201, 0.025° angular resolution, 5 kHz polling; Novotechnik) used in conjunction with a magnet (Z-RFC-P04; Novotechnik) embedded in the center of the rotating disk. A mirror (width 200 mm, height 140 mm) was placed underneath the disk at a 45° angle to reflect an image of the underside of a head-fixed mouse onto a high-speed CCD camera (RM-6740CL; JAI). The camera was equipped with a wide-angle lens (Xenoplan 1.4/8; Schneider-Kreuznach) and set to acquire frames (width 512 pixels, height 256 pixels) at a rate of 100 Hz using a custom-written LabView (National Instruments) acquisition program. Two flexible LED strips (Solarox LED strip 50 cm IR 940 nm, catalog number 500083094001; connector plug, catalog number 7090; powered by a 12V, 500 mA stabilized adaptor), one attached to the top edge of the mirror and the other on a

post facing the disk edge, were used to illuminate the mouse from below. A shaft-mounted computer-controlled electromagnetic clutch (Magneta; catalog number 14.100.01.30) allowed presentation of sensory perturbations to the mouse when briefly engaged.

For descriptions of two-photon microscopy, optogenetics, and behavioral tracking, as well as analysis of gait, please refer to the Supplemental Experimental Procedures.

SUPPLEMENTAL INFORMATION

Supplemental Information includes Supplemental Experimental Procedures, four figures, two tables, and three movies and can be found with this article online at http://dx.doi.org/10.1016/j.cub.2015.03.009.

AUTHOR CONTRIBUTIONS

T.M.H. conceived the disk treadmill, performed the experiments, and analyzed the data using custom-written scripts; J.R.G. developed custom acquisition and behavioral analysis software and the hyperacuity algorithm and analyzed the data; L.W. and C.C. advised on and contributed hardware to the optogenetic experiments. T.M.H, J.R.G., and C.I.D.Z. wrote the manuscript. C.I.D.Z. coordinated the project. All authors contributed to the final version of this manuscript.

ACKNOWLEDGMENTS

We are greatly indebted to J. Bos for assistance with the development and implementation of the disk treadmill. We further thank H. Hoedemaker and N. Flierman for experimental assistance and J. Plugge for help with data processing. This work was supported by the Dutch Organization for Medical Sciences (ZonMw; C.I.D.Z.), Behavioral Sciences (MAGW; C.I.D.Z.), and Life Sciences (ALW; C.I.D.Z.); Senter (Neuro-Basic; C.I.D.Z.); and ERC-adv of the European Community (C.I.D.Z.).

Received: January 6, 2015
Revised: February 18, 2015
Accepted: March 6, 2015
Published: April 2, 2015

REFERENCES

1. Flourens, P. (1842). Recherches Expérimentales sur les Propriétés et les Fonctions du Système Nerveux Donts les Animaux Vertébrés. (Paris: Crevot).
2. Babinski, J. (1899). De l'asynergie cérébelleuse. Rev. Neurol. (Paris) *7*, 806–816.
3. Thach, W.T., Goodkin, H.P., and Keating, J.G. (1992). The cerebellum and the adaptive coordination of movement. Annu. Rev. Neurosci. *15*, 403–442.
4. Welsh, J.P., Lang, E.J., Suglhara, I., and Llinás, R. (1995). Dynamic organization of motor control within the olivocerebellar system. Nature *374*, 453–457.
5. Llinas, R. (1964). Mechanisms of supraspinal actions upon spinal differences between reticular and cerebellar inhibitory actions upon alpha extensor motoneurons. J. Neurophysiol. *27*, 1117–1126.
6. Esposito, M.S., Capelli, P., and Arber, S. (2014). Brainstem nucleus MdV mediates skilled forelimb motor tasks. Nature *508*, 351–356.
7. Azim, E., Jiang, J., Alstermark, B., and Jessell, T.M. (2014). Skilled reaching relies on a V2a propriospinal internal copy circuit. Nature *508*, 357–363.
8. Allen, G.I., and Tsukahara, N. (1974). Cerebrocerebellar communication systems. Physiol. Rev. *54*, 957–1006.
9. Bastian, A.J., Martin, T.A., Keating, J.G., and Thach, W.T. (1996). Cerebellar ataxia: abnormal control of interaction torques across multiple joints. J. Neurophysiol. *76*, 492–509.
10. Eccles, J.C., Llinás, R., and Sasaki, K. (1966). The excitatory synaptic action of climbing fibres on the Purkinje cells of the cerebellum. J. Physiol. *182*, 268–296.
11. Vinueza Veloz, M.F., Zhou, K., Bosman, L.W.J., Potters, J.-W., Negrello, M., Seepers, R.M., Strydis, C., Koekkoek, S.K.E., and De Zeeuw, C.I. (2014). Cerebellar control of gait and interlimb coordination. Brain Struct. Funct. Published online August 20, 2014. http://dx.doi.org/10.1007/s00429-014-0870-1.
12. Badura, A., Schonewille, M., Voges, K., Galliano, E., Renier, N., Gao, Z., Witter, L., Hoebeek, F.E., Chédotal, A., and De Zeeuw, C.I. (2013). Climbing fiber input shapes reciprocity of Purkinje cell firing. Neuron *78*, 700–713.
13. Sánchez-Campusano, R., Gruart, A., and Delgado-García, J.M. (2009). Dynamic associations in the cerebellar-motoneuron network during motor learning. J. Neurosci. *29*, 10750–10763.
14. Sánchez-Campusano, R., Gruart, A., and Delgado-García, J.M. (2011). Timing and causality in the generation of learned eyelid responses. Front. Integr. Neurosci. *5*, 39.
15. de Zeeuw, C.I., Holstege, J.C., Ruigrok, T.J., and Voogd, J. (1989). Ultrastructural study of the GABAergic, cerebellar, and mesodiencephalic innervation of the cat medial accessory olive: anterograde tracing combined with immunocytochemistry. J. Comp. Neurol. *284*, 12–35.
16. Oscarsson, O. (1979). Functional units of the cerebellum-sagittal zones and microzones. Trends Neurosci. *2*, 144–145.
17. Ruigrok, T.J.H., Pijpers, A., Goedknegt-Sabel, E., and Coulon, P. (2008). Multiple cerebellar zones are involved in the control of individual muscles: a retrograde transneuronal tracing study with rabies virus in the rat. Eur. J. Neurosci. *28*, 181–200.
18. Llinás, R., and Sasaki, K. (1989). The Functional Organization of the Olivo-Cerebellar System as Examined by Multiple Purkinje Cell Recordings. Eur. J. Neurosci. *1*, 587–602.
19. De Gruijl, J.R., Hoogland, T.M., and De Zeeuw, C.I. (2014). Behavioral correlates of complex spike synchrony in cerebellar microzones. J. Neurosci. *34*, 8937–8947.
20. Ozden, I., Dombeck, D.A., Hoogland, T.M., Tank, D.W., and Wang, S.S.-H. (2012). Widespread state-dependent shifts in cerebellar activity in locomoting mice. PLoS ONE *7*, e42650.
21. Flusberg, B.A., Nimmerjahn, A., Cocker, E.D., Mukamel, E.A., Barretto, R.P.J., Ko, T.H., Burns, L.D., Jung, J.C., and Schnitzer, M.J. (2008). High-speed, miniaturized fluorescence microscopy in freely moving mice. Nat. Methods *5*, 935–938.
22. Ghosh, K.K., Burns, L.D., Cocker, E.D., Nimmerjahn, A., Ziv, Y., Gamal, A.E., and Schnitzer, M.J. (2011). Miniaturized integration of a fluorescence microscope. Nat. Methods *8*, 871–878.
23. Llinás, R. (1974). Eighteenth Bowditch lecture. Motor aspects of cerebellar control. Physiologist *17*, 19–46.
24. Green, M., and Sidman, L. (1962). Tottering—a neuromusclar mutation in the mouse. And its linkage with oligosyndacylism. J. Hered. *53*, 233–237.
25. Noebels, J.L., and Sidman, R.L. (1979). Inherited epilepsy: spike-wave and focal motor seizures in the mutant mouse tottering. Science *204*, 1334–1336.
26. Kaplan, B.J., Seyfried, T.N., and Glaser, G.H. (1979). Spontaneous polyspike discharges in an epileptic mutant mouse (tottering). Exp. Neurol. *66*, 577–586.
27. Wakamori, M., Yamazaki, K., Matsunodaira, H., Teramoto, T., Tanaka, I., Niidome, T., Sawada, K., Nishizawa, Y., Sekiguchi, N., Mori, E., et al. (1998). Single tottering mutations responsible for the neuropathic phenotype of the P-type calcium channel. J. Biol. Chem. *273*, 34857–34867.
28. Witter, L., Canto, C.B., Hoogland, T.M., de Gruijl, J.R., and De Zeeuw, C.I. (2013). Strength and timing of motor responses mediated by rebound firing in the cerebellar nuclei after Purkinje cell activation. Front. Neural Circuits *7*, 133.

29. Crone, S.A., Zhong, G., Harris-Warrick, R., and Sharma, K. (2009). In mice lacking V2a interneurons, gait depends on speed of locomotion. J. Neurosci. *29*, 7098–7109.

30. Barski, J.J., Dethleffsen, K., and Meyer, M. (2000). Cre recombinase expression in cerebellar Purkinje cells. Genesis *28*, 93–98.

31. Hartigan, J.A., Hartigan, P.M., Annals, T., and Mar, N. (2007). The dip test of unimodality. Ann. Stat. *13*, 70–84.

32. Dombeck, D.A., Khabbaz, A.N., Collman, F., Adelman, T.L., and Tank, D.W. (2007). Imaging large-scale neural activity with cellular resolution in awake, mobile mice. Neuron *56*, 43–57.

33. Jiménez-Díaz, L., Navarro-López, J. de D., Gruart, A., and Delgado-García, J.M. (2004). Role of cerebellar interpositus nucleus in the genesis and control of reflex and conditioned eyelid responses. J. Neurosci. *24*, 9138–9145.

34. Makarenko, V., and Llinás, R. (1998). Experimentally determined chaotic phase synchronization in a neuronal system. Proc. Natl. Acad. Sci. USA *95*, 15747–15752.

35. Leznik, E., Makarenko, V., and Llinás, R. (2002). Electrotonically mediated oscillatory patterns in neuronal ensembles: an in vitro voltage-dependent dye-imaging study in the inferior olive. J. Neurosci. *22*, 2804–2815.

36. Chorev, E., Yarom, Y., and Lampl, I. (2007). Rhythmic episodes of subthreshold membrane potential oscillations in the rat inferior olive nuclei in vivo. J. Neurosci. *27*, 5043–5052.

37. Montarolo, P.G., Palestini, M., and Strata, P. (1982). The inhibitory effect of the olivocerebellar input on the cerebellar Purkinje cells in the rat. J. Physiol. *332*, 187–202.

38. Hoebeek, F.E., Stahl, J.S., van Alphen, A.M., Schonewille, M., Luo, C., Rutteman, M., van den Maagdenberg, A.M., Molenaar, P.C., Goossens, H.H., Frens, M.A., and De Zeeuw, C.I. (2005). Increased noise level of purkinje cell activities minimizes impact of their modulation during sensorimotor control. Neuron *45*, 953–965.

39. Blenkinsop, T.A., and Lang, E.J. (2006). Block of inferior olive gap junctional coupling decreases Purkinje cell complex spike synchrony and rhythmicity. J. Neurosci. *26*, 1739–1748.

40. Lefler, Y., Yarom, Y., and Uusisaari, M.Y. (2014). Cerebellar inhibitory input to the inferior olive decreases electrical coupling and blocks subthreshold oscillations. Neuron *81*, 1389–1400.

41. Freeze, B.S., Kravitz, A.V., Hammack, N., Berke, J.D., and Kreitzer, A.C. (2013). Control of basal ganglia output by direct and indirect pathway projection neurons. J. Neurosci. *33*, 18531–18539.

42. Ayling, O.G.S., Harrison, T.C., Boyd, J.D., Goroshkov, A., and Murphy, T.H. (2009). Automated light-based mapping of motor cortex by photoactivation of channelrhodopsin-2 transgenic mice. Nat. Methods *6*, 219–224.

43. Khosrovani, S., Van Der Giessen, R.S., De Zeeuw, C.I., and De Jeu, M.T.G. (2007). In vivo mouse inferior olive neurons exhibit heterogeneous subthreshold oscillations and spiking patterns. Proc. Natl. Acad. Sci. USA *104*, 15911–15916.

Current Biology

Supplemental Information

Role of Synchronous Activation of Cerebellar Purkinje Cell Ensembles in Multi-joint Movement Control

Tycho M. Hoogland, Jornt R. De Gruijl, Laurens Witter, Cathrin B. Canto, and Chris I. De Zeeuw

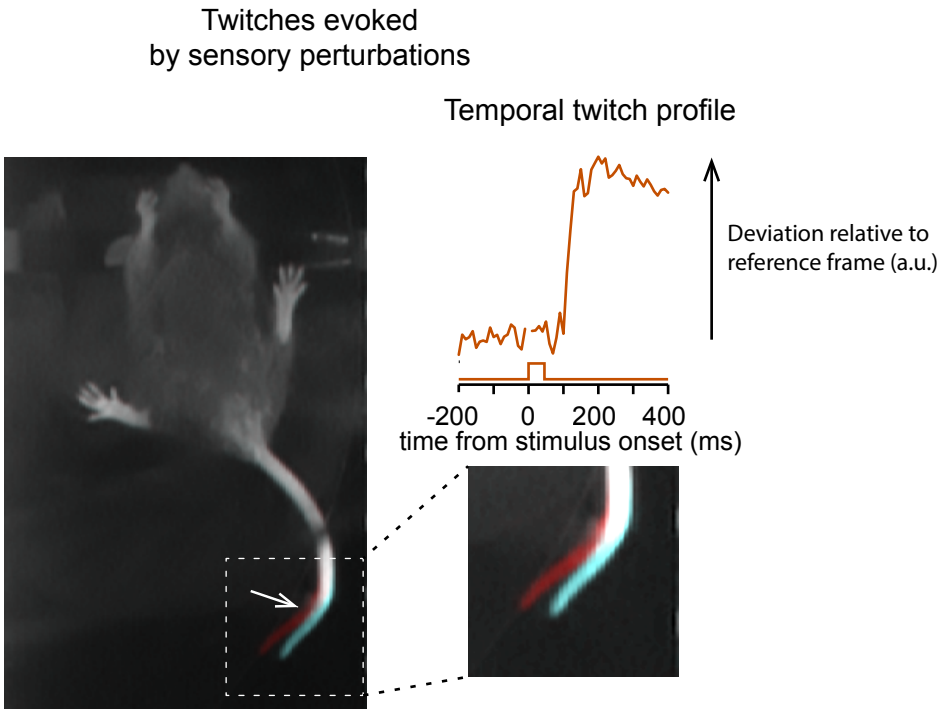
Twitches evoked
by sensory perturbations
Temporal twitch profile
Deviation relative to
reference frame (a.u.)
-200
0
200
400
time from stimulus onset (ms)

Figure S1

Figure S1, related to Figure 1. Sensory perturbations evoked using a magnetic clutch along the axis of a disk treadmill

Brief sensory perturbations could be applied using an electromagnetic coupling device (clutch) along the treadmill axis to which mice responded with brief twitches of limbs and tail (inset and arrow indicating predominant tail twitch in this example). The frame difference in this example was between the frame corresponding to the stimulus offset (cyan) and a frame 130 ms later (red) to show tail displacement. A custom algorithm [S1] was used to generate twitch profiles in response to the sensory perturbation and conveyed information about twitch onset.

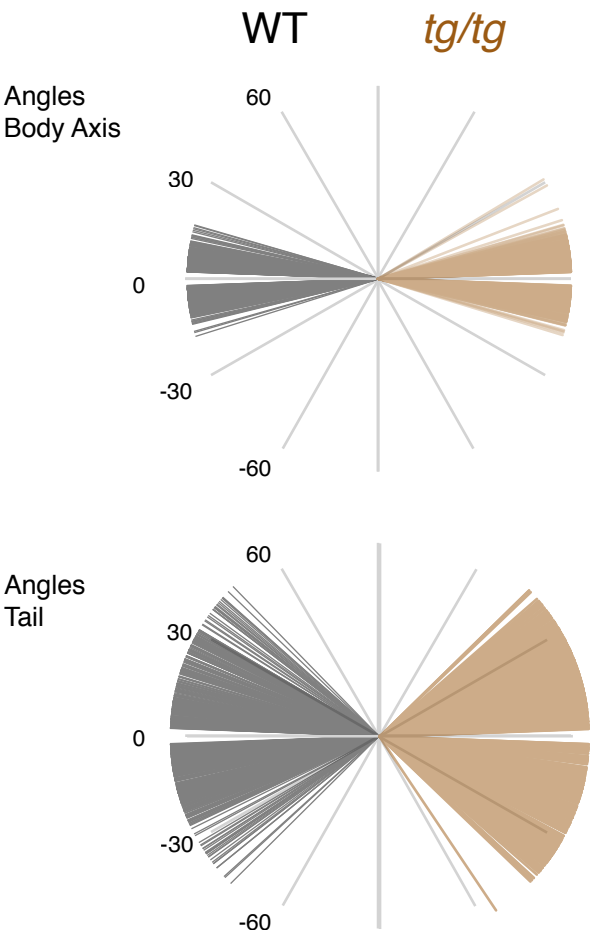

Figure S2

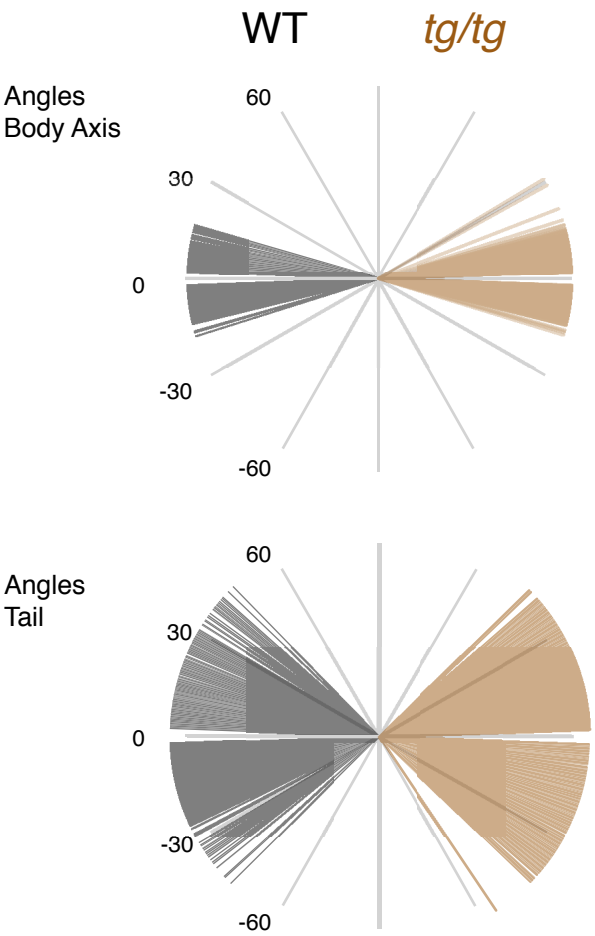

Figure S2

Figure S2, related to Figure 2. Plot of the body axis and tail angles in wild type and tottering (*tg/tg*) mice during locomotion

Top: body axis angles for wild type (left) and *tg/tg* mice (right). Bottom: tail axis angles for wild type (left) and *tg/tg* mice (right).

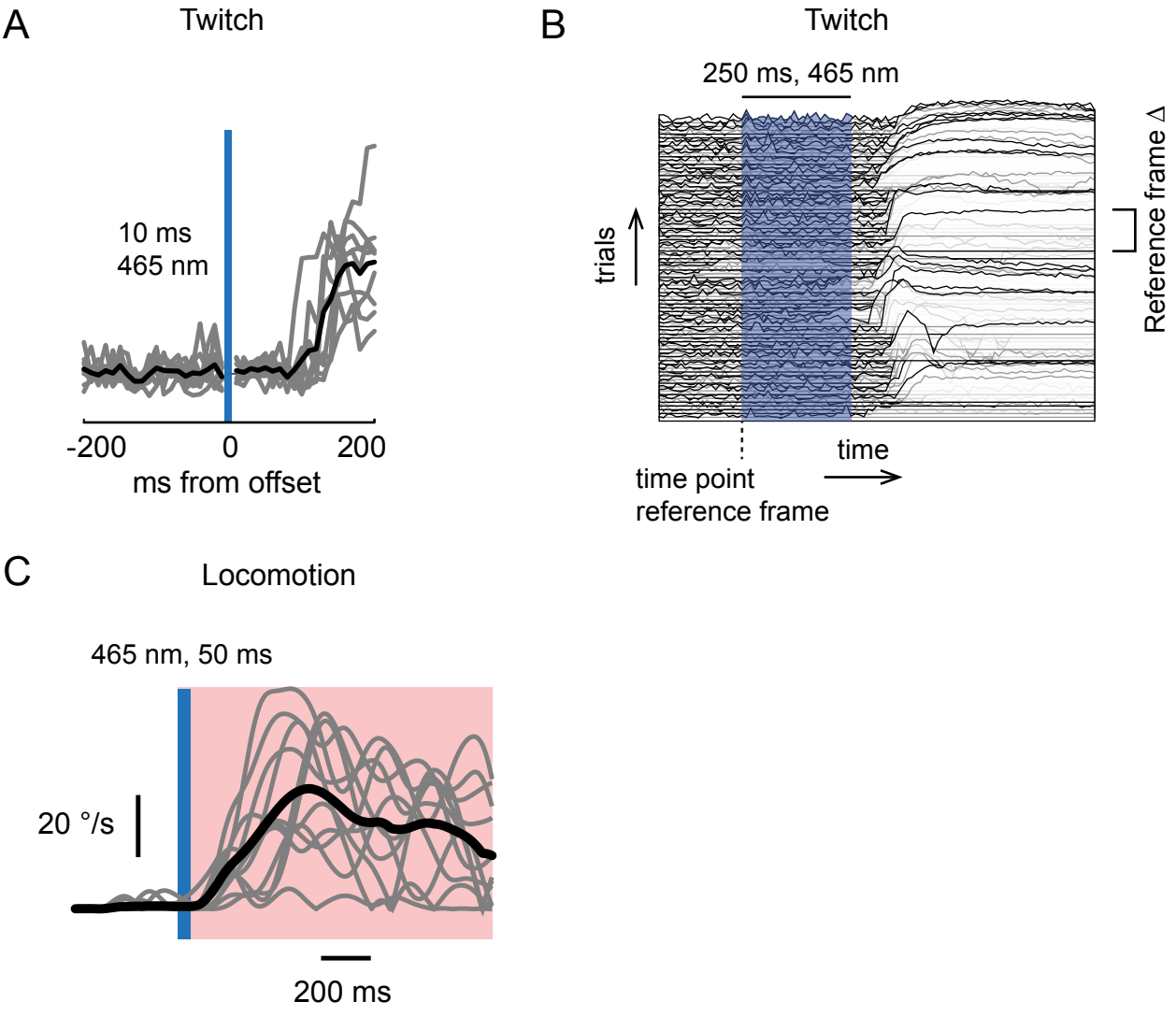
A
Twitch
10 ms
465 nm
-200
0
200
ms from offset
B
Twitch
250 ms, 465 nm
trials
Reference frame Δ
time
time point
reference frame
C
Locomotion
465 nm, 50 ms
20 °/s
200 ms

Figure S3

Figure S3, related to Figure 3. Timing of twitches evoked by optogenetic activation of Purkinje cells

(A) Optogenetic activation of PCs for durations as short as 10 ms were sufficient to trigger a behavioral response comprising twitches. Shown are individual responses within a single experiment (gray) and the population average (black). (B) Temporal profiles of twitch responses following a 250 ms duration stimulus demonstrating that optogenetic activation of PCs during rest can evoke twitch responses that follow the offset of a light stimulus.

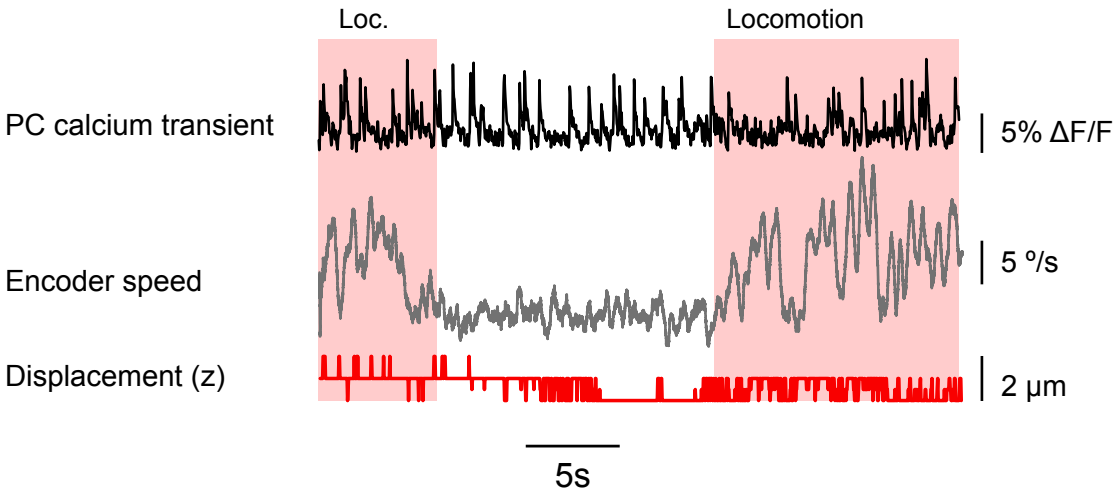
Loc.
Locomotion
PC calcium transient
5% ΔF/F
Encoder speed
5 °/s
Displacement (z)
2 µm
5s

Figure S4

Figure S4, related to Experimental Procedures. Axial movement during two-photon imaging on a disk treadmill

Shown are calcium transients recorded from a Purkinje cell (PC), disk encoder speed and axial displacement. Axial displacement was calculated by acquiring a z-stack of images at 1μm intervals when an animal was at rest. Frames obtained during locomotion from a single optical plane were cross-correlated with the reference images at different depths obtained at rest to calculate displacement.

Table S1. Stance and swing durations in wild type and tottering mice.

	WT stance (mean±sd)	*tg/tg* stance (mean±sd)	WT swing (mean±sd)	*tg/tg* swing (mean±sd)
LF	304±113 ms	325±115 ms	200±69 ms	246±106 ms
RF	277±149 ms	263±125 ms	222±88 ms	265±85 ms
LH	313±147 ms	286±186 ms	208±117 ms	214±96 ms
RH	320±165 ms	282±156 ms	221±71 ms	262±126 ms
	WT vs. *tg/tg* stance (Kruskal-Wallis): $p=0.06$		WT vs. *tg/tg* swing (Kruskal-Wallis): $p=1.3*10^{-11}$	
	WT stance vs. swing (Kruskal-Wallis): $p=1.9*10^{-62}$		*tg/tg* stance vs. swing (Kruskal-Wallis): $p=5.6*10^{-11}$	

Table S2. Properties of complex spike elicited calcium transients in PC dendrites of wild type and tottering mice.

	WT (mean±sd), median	*Tg/tg* (mean±sd), median	P-value	Type of test
Amplitude ΔF/F %	6.5±2.6, 6.2 (7354 transients)	4.7±1.5, 4.5 (2624 transients)	$p=2.7*10^{-234}$	K-S, 2-sample
$t_{1/2}$ (ms)	112.3±38.7, 106.7 (7354 transients)	100.1±37.5, 94.0 (2624 transients)	$p=6.5*10^{-52}$	K-S, 2-sample
Rates rest	1.13±0.4, 1.17 (630 dendrites)	1.26±0.4, 1.23 (192 dendrites)	P=0.001	K-S, 2-sample
Rates locomotion	1.43±0.3Hz, 1.40Hz (630 dendrites)	1.52±0.3Hz, 1.55Hz (192 dendrites)	$p=7.9*10^{-07}$	K-S, 2-sample

Supplemental Experimental Procedures

Two-photon microscopy

A two-photon microscope (TrimScope II, Lavision BioTec, Bielefeld, Germany) was used in combination with a Chameleon Ultra II pulsed infrared laser (pulse width: 140 fs, reptition rate: 80 MHz; Coherent, Santa Ana, California) to image microcircuits in the cerebellum. All imaging was performed using a 20x, 1.0 N.A. objective (XLUMPLSLN, Olympus, Tokyo, Japan). Images were acquired with sample times of 15 ms and 30 ms per frame. A hyperacuity algorithm was applied to detect CS events triggered off of sensory perturbations, or locomotion onsets to realign events with ms precision [S2]. Imaging was done in the molecular layer of the mouse cerebellum (50-100 μm depth) where CFs trigger CS-mediated calcium transients in PC dendrites. PC CSs were imaged using the synthetic fluorescent calcium indicator Oregon Green BAPTA-1/AM (Life Technologies, Carlsbad, California), which was bolus-loaded into the cerebellar cortex [S3]. Recordings began at least 30 minutes after loading. CS-mediated calcium transients were extracted from PCs in two steps. A median filter with 3 by 3 pixel kernel was applied to all two-photon image frames prior to spatial independent component analysis with the resulting spatial components being used to segment responding PC dendrites [S4]. A threshold consisting of the mean pixel intensity plus five standard deviations was applied to each component. Overlapping pixels were removed and small objects below a size threshold (< 15 pixels) discarded. Fluorescence was averaged over all the pixels contained within each segmented PC dendrite. $\Delta F/F$ was calculated as described previously [S3].

Calcium transients were high-pass filtered to remove slow baseline fluctuations. Subsequently CS event extraction was performed using a spike train inference algorithm [S5].

Optogenetics

The PC specific PCP2-Cre driver line (The Jackson Laboratory, Maine, JAX # 004146) was crossed with ChR2(H134R)-eYFP mice (Madisen et al., 2012, JAX # 012569). Expression of the L7-ChR2(H134R)-eYFP fusion protein. Craniotomies were made above vermis lobule V. A 400 µm multimode optical fiber (Thorlabs, New Jersey) was placed just above the surface of the cerebellum and secured with Kwik-Sil (World Precision Instruments, Sarasota, Florida) and dental cement (Super-Bond C&B, Sun-Medical, Moriyama City, Japan). A custom LED driver was used to control the output power of the LED [S1]. In our experiments we used 1-3 mW output power as measured coming out of the fiber tip. For the fiber used this corresponded with ~8-4 mW/mm^2 (1 mW, from surface to Purkinje cell layer) to ~24-13 mW/mm^2 (3 mW, from surface to Purkinje cell layer) and has been shown using whole-cell recordings in vivo to increase SS firing rate in PCs [S1].

Behavioral tracking

The Matlab code used for the gait tracking analysis, determination of body/tail axis angles and calculation of temporal twitch profiles has been deposited at: https://github.com/CCCgroup/Tracking. Whole body twitches evoked by sensory perturbations through engagement of the magnetic clutch were analyzed using a custom algorithm described before in detail [S1].

Analysis of gait

The objects in our monochrome camera data change position, size and shape. Since mice were head-fixed in the setup, standard algorithms for freely moving animals could not be used, as these generally assume constant locations for limbs during stance. Standard blob tracking algorithms for objects moving through frames often use parameters such as size and shape to track targets. In order to detect limb movements and locomotion, we developed a gait tracking application in Matlab (MathWorks, Natick, Massachusetts). As a pre-processing step all frames were denoised using the software CANDLE [S6]. Subsequently, background subtraction was performed on all frames to facilitate object detection. Changes in pixel values between frames were calculated by taking the sum of the absolute value of a subtraction of two consecutive frames. The second frame of pairs of subsequent frames of which the pixel difference values exceeded a threshold of the mean plus one standard deviation were selected to generate a background image. A pixel intensity threshold for object detection as well as a minimum object size criterion were set manually. Thresholded objects were matched between frames, based on the in-frame center-of-mass coordinates and the number of pixels constituting the object. If the distance between the centers of mass exceeded a set threshold (20 pixels, ~ 7 mm) or if the number of pixels changed more than 10% from one frame to the next, a putative match was deemed invalid. If multiple objects were eligible for matching, the closest (Euclidian distance) match was selected. This processing stage generated a set of object trace snippets in which objects were not yet classified, but already temporally linked for a limited sequence of

frames. For object classification, a feed-forward three-layer neural network was used (Neural Network Toolbox) and a training set was generated by taking a selection of 15% of the frames (with a minimum of 150 and a maximum of 500 that always included those frames that were used for rendering the background image and were supplemented with randomly selected frames). The frames used for generating the background image were explicitly included, as these images likely represent the most problematic cases for a trained classifier if such cases were not sufficiently represented in the data set it was trained on. The objects detected in the training set were manually assigned to any of six classes: tail, left hind limb (LH), right hind paw (RH), left front paw (LF), right front paw (RF) and unclassified. The results of this classification were extended to the trace snippets and the neural network was trained on the data, using the following parameters: object size, center-of-mass coordinates, and orientation. The trained network was used to perform a final classification on the entire data set. Following this automated classification, the results were manually inspected and incorrectly classified objects were removed on a frame-by-frame basis. Paw objects moving in the direction of the disk as judged by the magnetic encoder signal were considered as being “in stance”. If the direction of a paw object’s motion ran counter to that of the disc, it was considered to be “in swing”. From the final object set several gait parameters were extracted including stride length and duration.

Supplemental References

S1 Witter, L., Canto, C. B., Hoogland, T. M., de Gruijl, J. R., and De Zeeuw, C. I. (2013). Strength and timing of motor responses mediated by rebound firing in the cerebellar nuclei after Purkinje cell activation. Front. Neural Circuits *7*, 133, 1–14.

S2 De Gruijl, J. R., Hoogland, T. M., and De Zeeuw, C. I. (2014). Behavioral correlates of complex spike synchrony in cerebellar microzones. J. Neurosci. *34*, 8937–47.

S3 Ozden, I., Dombeck, D. A., Hoogland, T. M., Tank, D. W., and Wang, S. S.-H. (2012). Widespread state-dependent shifts in cerebellar activity in locomoting mice. PLoS One *7*, e42650.

S4 Hyvärinen, a (1999). Fast and robust fixed-point algorithms for independent component analysis. IEEE Trans. Neural Netw. *10*, 626–34.

S5 Vogelstein, J. T., Packer, A. M., Machado, T. a, Sippy, T., Babadi, B., Yuste, R., and Paninski, L. (2010). Fast nonnegative deconvolution for spike train inference from population calcium imaging. J. Neurophysiol. *104*, 3691–704.

S6 Coupé, P., Munz, M., Manjón, J. V, Ruthazer, E. S., and Louis, D. (2012). A CANDLE for a deeper in vivo insight. Med. Image Anal. *16*, 849–864.

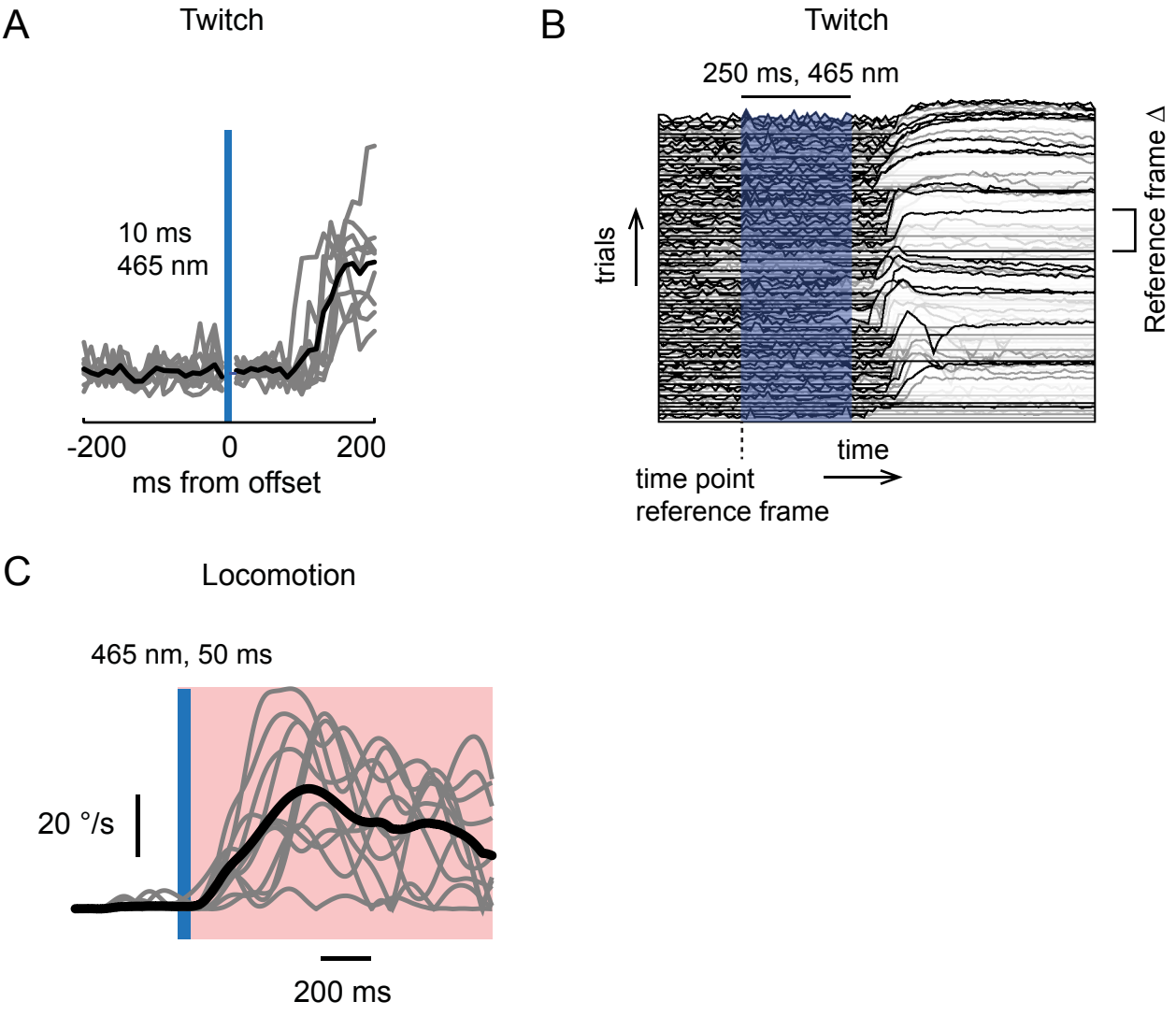
A
Twitch
10 ms
465 nm
-200
0
200
ms from offset
B
Twitch
250 ms, 465 nm
trials
Reference frame Δ
time
time point
reference frame
C
Locomotion
465 nm, 50 ms
20 °/s
200 ms

Figure S3

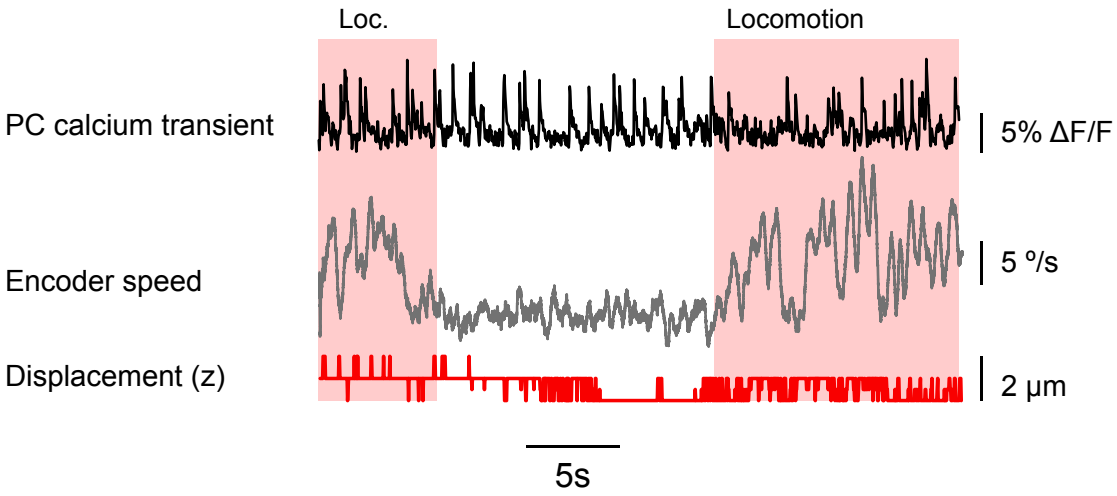
Loc.
Locomotion
PC calcium transient
5% ΔF/F
Encoder speed
5 °/s
Displacement (z)
2 µm
5s

Figure S4